1-1-2009

Optimization of nominal mixing ratio of Mg to B in fabrication of magnesium diboride bulk

Yun Zhang
University of Wollongong, yunz@uow.edu.au

Cheng Lu
University of Wollongong, chenglu@uow.edu.au

Sihai Zhou
University of Wollongong, sihai@uow.edu.au

Kookchae Chung
Korea Institute of Materials Science

Wenxian Li
University of Wollongong, wenxian@uow.edu.au

Optimization of Nominal Mixing Ratio of Mg to B in Fabrication of Magnesium Diboride Bulk

Yun Zhang, Cheng Lu, Si Hai Zhou, Kookchae Chung, and Wen Xian Li

***Abstract*—In this paper bulk magnesium diboride (Mg_xB_2) with x varying from 0.9 to 1.3 was prepared by solid state reaction. The Mg:B mixing ratio for ideal MgB_2 is 1:2. The samples were sintered at 800°C for 60 h. Quantitative X-ray diffraction (XRD) analysis was performed to obtain the lattice parameters, the microstrain, and the weight fraction of impurities using the Rietveld refinement method. It has been found that the fraction of pure MgB_2 phase increases from $x = 0.9$ to $x = 1.1$, and then decreases with further increases in x. $Mg_{1.1}B_2$ exhibits the highest critical current density, J_c, over other samples in both low fields and high fields. A direct correlation between J_c and connectivity indicates that better connectivity, caused by smaller amounts of impurities, results in the best J_c in $Mg_{1.1}B_2$.**

***Index Terms*—Connectivity, MgB_2, nominal mixing ratio, superconductivity.**

I. Introduction

MgB_2 is a promising metallic superconductor operating at relatively high temperatures around 20 K [1]. MgB_2 exhibits several prominent characteristics, including a high transition temperature, a simple crystal structure, abundance of the raw materials in nature, and the absence of weak intergranular links. However, the weak flux pinning, low critical current density (J_c) in high fields, and low irreversibility field (H_{irr}) are retarding its application. Numerous efforts have been focused on the improvement of J_c by chemical doping [2], [3], ball-milling methods [4], [5], thermo-mechanical processing methods [6]–[8], and proton irradiation [9].

It has been found that the stoichiometry of MgB_2 significantly affects the superconducting properties. Unfortunately, discrepancies on this topic still exist. Jiang *et al.* [10] reported that slightly Mg-deficient samples showed higher J_c in high fields, whereas samples with stoichiometric Mg or a slight excess of Mg exhibited better J_c in low fields. The reason for higher J_c in high fields was attributed to the enhanced grain boundary pinning caused by the smaller grain size. Perner *et al.* [11] found that the best critical temperature (T_c) and J_c were obtained for an Mg surplus of 5wt%. Chen *et al.* [12] reported that nominally Mg-deficient samples had enhanced in-field J_c values over samples prepared in an Mg excess environment. They attributed this to the increased structural disorder. In this paper, we systematically investigated the effects of the nominal mixing ratio of Mg to B, which was varied from 0.9:2 to 1.3:2, on the superconducting properties of Mg_xB_2. The Mg:B mixing ratio for ideal MgB_2 is 1:2. A detailed analysis of the fraction of each phase, the lattice parameters, microstrain, T_c, the upper critical field (H_{c2}), J_c, and connectivity has been conducted. It was found that the sample with $x = 1.1$ exhibited the highest J_c in all fields at 5 K and 20 K. A clear correlation between J_c and connectivity indicates that the good connectivity in the sample with 10% Mg excess caused the J_c enhancement in both low fields and high fields.

II. Experimental

Mg_xB_2 samples with $x = 0.9$, 1, 1.1, 1.2, and 1.3 were prepared by solid state reaction. Mg powder (1–11 μm) and amorphous boron powder (99%) were used as the starting materials. The powders were carefully mixed by grinding in a mortar and pressed into pellets 13 mm in diameter and about 2.5 mm thick. The pellets were sealed into Fe tubes. The sealed tubes were then heated in a tube furnace under pure Ar gas and sintered at 800°C for 60 h prior to cooling to room temperature.

The obtained MgB_2 samples were examined by X-ray diffraction (XRD) in a Philips PW1730 Model diffractometer using Cu $K\alpha$ radiation ($\lambda = 1.541838$ Å). The XRD patterns were collected over a 2θ range from 20° to 80° with a step size of 0.02°. Lattice parameter calculations and quantitative phase analysis were carried out based on the XRD patterns.

Magnetic measurements of the samples were conducted in a commercial Quantum Design Physical Properties Measurement System (PPMS) after they have been polished into a cuboid shape for measurements. Their dimensions were accurately measured with a digital micrometer. The DC magnetic response was obtained in an applied low field of 1 Oe using the conventional zero-field-cooled (ZFC) and field-cooled (FC) procedures. Magnetic hysteresis loops were measured at temperatures of 5 K and 20 K. The critical current density was calculated from the magnetization hysteresis loops, based on the dimensions of the samples. The resistivity was measured as a function of temperature and magnetic field, using a four probe resistance technique.

III. Results and Discussion

Fig. 1 shows the powder XRD patterns of Mg_xB_2 samples with $x = 0.9$, 1, 1.1, 1.2, and 1.3. All the major peaks of the

Manuscript received August 27, 2008. First published June 05, 2009; current version published July 15, 2009. This work was supported by the Australian Research Council.

Y. Zhang, S. H. Zhou, and W. X. Li are with the Institute for Superconducting and Electronic Materials, University of Wollongong, Wollongong, NSW 2522, Australia (e-mail: yz268@uow.edu.au).

C. Lu is with the School of Mechanical, Materials & Mechatronic Engineering, University of Wollongong, NSW, 2522, Australia (e-mail: chenglu@uow.edu.au).

K. C. Chung is with the New Energy Materials Group, Korea Institute of Materials Science, Changwon, Korea (e-mail: kcchung@kims.re.kr).

Color versions of one or more of the figures in this paper are available online at http://ieeexplore.ieee.org.

Digital Object Identifier 10.1109/TASC.2009.2017700

TABLE I
REFINED PARAMETERS IN Mg_xB_2

Samples	R_{wp}(%)	Weight fraction (%)				Lattice Parameters (Å)		Microstrain (%)
		MgB_2	MgO	MgB_4	Mg	a	c	
$Mg_{0.9}B_2$	7.48	69.03	7.06	23.91		3.085	3.526	0.201
MgB_2	5.87	73.2	7.53	19.27		3.084	3.525	0.167
$Mg_{1.1}B_2$	6.05	90.03	9.97			3.084	3.525	0.216
$Mg_{1.2}B_2$	6.38	88.73	10.4		0.87	3.085	3.523	0.185
$Mg_{1.3}B_2$	6.202	85.07	12.67		2.25	3.084	3.519	0.229

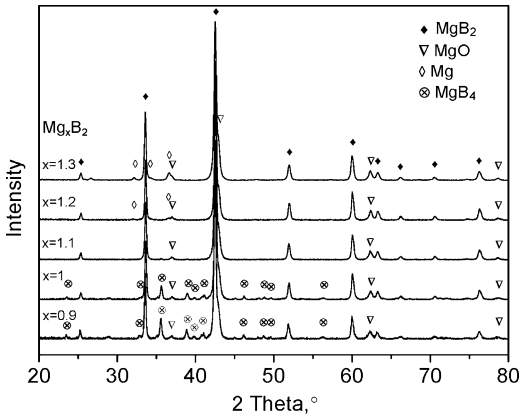

Fig. 1. Powder XRD traces of Mg_xB_2 samples with x = 0.9, 1, 1.1, 1.2, and 1.3.

MgB_2 hexagonal structure (space group P6/mmm) can be identified, indicating that the samples mainly consisted of the desired MgB_2 phase. Besides MgB_2, the impurity MgO existed in all the samples. Two strong peaks of the MgO phase are located at $2\theta \approx 42.96°$ and $2\theta \approx 62.28°$. Another two weaker peaks at $2\theta \approx 36.80°$ and $2\theta \approx 78.54°$ can also be observed in the XRD patterns. MgO impurities could be formed by reactions during the sintering process. The reacting oxygen could be introduced from the air trapped in the tubes and also from oxygen in the starting boron powers. For the samples with $x < 1.1$, MgB_4 was detected. MgB_4 exists due to a deficiency of magnesium, which is caused by evaporation of the magnesium and formation of MgO. At $x = 1.1$, MgB_4 disappears, and only MgO impurities can be observed. When x further increases to 1.2, magnesium metal becomes excessive. Therefore, two major peaks of magnesium metal are displayed in the XRD patterns of $Mg_{1.2}B_2$ and $Mg_{1.3}B_2$ at $2\theta \approx 36.62°$ and $2\theta \approx 32.12°$.

Rietveld refinement was performed to analyze the XRD measurements. The refinable parameters include the weight fraction of each phase, the lattice parameters of MgB_2, and the percentage of microstrain. A measure of similarity (R_{wp}) between the measured diffraction patterns and the simulated diffraction patterns is shown in Table I. A low R_{wp} indicates good agreement between the measured and simulated data. All the R_{wp} values are below 7.5%. This indicates that the calculated results are acceptable. The calculated weight fraction of each phase in the samples is also listed in Table I. It was found that the weight fraction of pure MgB_2 phase increased from $x = 0.9$ to $x = 1.1$, and then decreased. There are large differences in the weight fraction of MgB_2 phase in the samples, varying from 69.03% to 90.03%. The weight fraction of MgO increases with x. A large amount of MgB_4 phase exists in MgB_2 and $Mg_{0.9}B_2$. Its weight fraction increases with decreasing x. It seems that the existence of MgB_4 significantly reduces the weight fraction of MgB_2 phase. A small amount of Mg appears in the samples with sufficient Mg precursor powder ($Mg_{1.2}B_2$ and $Mg_{1.3}B_2$). Its fraction increases with x.

The calculated in-plane lattice constant (a) in the samples is nearly the same. The inter-plane lattice constant (c) decreases from 3.526 Å to 3.519 Å with increasing x. The lattice constant c of $Mg_{0.9}B_2$ is larger than the value for the ideal MgB_2 structure $(c = 3.521$ Å). This indicates that a large amount of vacancies exist in the sample. This can be attributed to the nominal deficiency of magnesium in $Mg_{0.9}B_2$ and the formation of MgO. For the sample with stoichiometric Mg $(x = 1)$, the Mg deficiency and the vacancies still exist, due to the formation of MgO. As the nominal ratio of Mg to B (x:2) increases, the nominal or real deficiency of Mg decreases. Therefore, the vacancies in the samples are reduced, resulting in a decreased c, as depicted in Table I. In the $Mg_{1.3}B_2$ sample, the magnesium deficiency disappears, and boron becomes more than sufficient. The redundant boron atoms may diffuse into the MgB_2 lattice as interstitial atoms, leading to a smaller lattice parameter c than the ideal value $(c = 3.521$ Å).

Table I also shows that microstrain varies from 0.167% to 0.229%. $Mg_{1.3}B_2$ has the largest microstrain, while MgB_2 exhibits the smallest one. Microstrain does not monotonically vary with the nominal ratio of Mg to B. The reason can be attributed to the effect of the MgB_4 and Mg impurities. The existence of the impurity can change microstrain. MgB_4 appears in $Mg_{0.9}B_2$ and MgB_2 and its amount decreases with x, while the metal Mg phase exists in $Mg_{1.2}B_2$ and $Mg_{1.3}B_2$ and its amount increases with x. The variation of amount of these impurities produces a complicated relationship between microstrain and the nominal ratio of Mg to B.

Fig. 2 shows a plot of the magnetic susceptibility against the temperature in an applied field of $H = 1$ Oe for zero field cooled samples. The magnetic susceptibility for the field cooled condition is not displayed in the figure, since the values are very close

TABLE II
PROPERTIES OF Mg_xB_2

Samples	T_c (K)	J_c at 0T and 20K (Acm^{-2})	J_c at 4.6T and 20K (Acm^{-2})	ρ_{40K} ($\mu\Omega cm$)	ρ_{300K} ($\mu\Omega cm$)	A_F	H_{c2} at 20k (T)
$Mg_{0.9}B_2$	37.88	170399	137	50.38	106.51	0.130	9.24
MgB_2	37.62	228777	147	31.51	70.42	0.188	8.69
$Mg_{1.1}B_2$	37.55	397933	1042	22.48	51.44	0.252	9.4
$Mg_{1.2}B_2$	37.53	374204	226	21.49	53.79	0.226	9.18
$Mg_{1.3}B_2$	37.39	366490	157	23.57	57.87	0.213	9.71

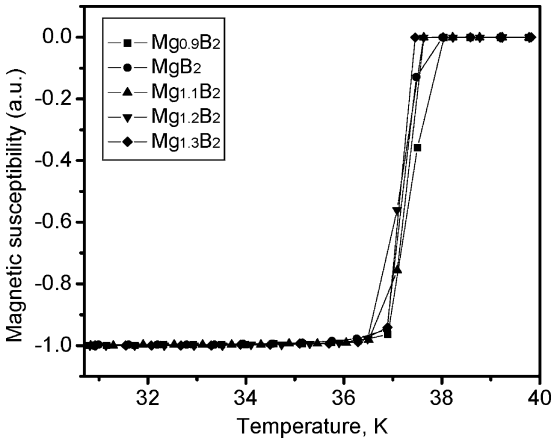

Fig. 2. Magnetic susceptibility plotted against temperature.

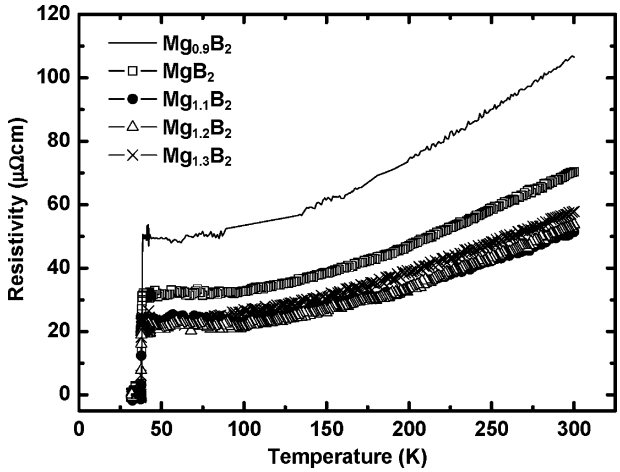

Fig. 3. Resistivity versus temperature for the samples.

to zero. This demonstrates that the flux pinning force in all the samples is quite large. The critical temperature (T_c) is defined as the temperature corresponding to the onset of diamagnetism, and the transition width (ΔT_c) is defined as the temperature variation between 10% and 90% of the full drop in the magnetic susceptibility. From Table II it can be seen that T_c is similar for all the samples within a range of 0.5 K, which is consistent with the observations of Chen *et al.* [12]. T_c slightly decreases with x. It also linearly decreases with the lattice parameter *c*. A decrease in the lattice parameters reduces the electronic density of states (DOS) at the Fermi level and hardens the optical E_{2g} phonons [13]. The reduction in the DOS and the hardening of the E_{2g} phonons depress T_c. ΔT_c in all the samples is sharp, with a width of $\sim$1 K as shown in Fig. 2. This indicates that the MgB_2 phase is quite homogeneous.

The resistivity (ρ) results are shown in Fig. 3. It can be observed that the resistivities in the samples with $x \geq 1.1$ are close to each other. The resistivity increases as x decreases from 1.1 to 0.9. The resistivities at 40 K and 300 K ($\rho_{40\,K}$ and $\rho_{300\,K}$) were collected from Fig. 3 and are listed in Table II. $Mg_{1.2}B_2$ has the smallest $\rho_{40\,K}$, while $\rho_{300\,K}$ in $Mg_{1.3}B_2$ is smallest. All $\rho_{40\,K}$s are higher than for single crystal (5.3 $\mu\Omega cm$, [14]) and for dense filaments made by chemical vapor deposition (CVD) (7.3 $\mu\Omega cm$, [15]). The reason can be attributed to poor connectivity in the studied samples. The XRD traces in Fig. 1 show the presence of a large amount of MgO in the samples. MgO is mainly present in the grain boundaries as an insulator, which reduces the effective cross-sectional area of the samples and then increases the resistivity. The impurity MgB_4 also increases the resistivity in $Mg_{0.9}B_2$ and MgB_2. The presence of Mg metal can reduce the resistivity, since Mg is a good conductor. However, the influence of Mg is not significant because its amount is quite small. The effective cross-sectional area (A_F) can be estimated from the equation, $A_F = \Delta\rho_{ideal}/(\rho_{300\,K} - \rho_{40\,K})$, which was proposed by Rowell [16]. $\Delta\rho_{ideal}$ is the ideal change in resistivity from 300 K to 40 K for a fully connected sample. It was set to be 7.3 $\mu\Omega cm$ according to [17]. The calculated A_F is displayed in Table II. A_F varies from 0.13 to 0.252, indicating poor connection in the samples. It can be noted from Tables I and II that A_F is related to the weight fraction of the MgB_2 phase. This reveals that the poor connectivity is mainly caused by the impurities.

The critical current density was calculated from the measured magnetization hysteresis loops, with the calculation based on the Bean model. Critical current densities at 5 K and 20 K are shown in Fig. 4. J_c in the flux jumping region is not shown in the figure. It is clear that $Mg_{1.1}B_2$ has the maximum J_c for all the fields at both 5 K and 20 K. This means that 1.1:2 is the optimum nominal mixing ratio of Mg to B under current processing conditions. The $Mg_{0.9}B_2$ sample has the lowest J_c.

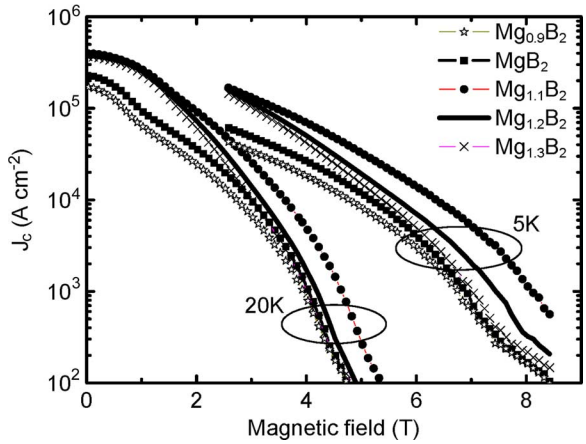

Fig. 4. Magnetic field dependence of critical current density in Mg_xB_2 at the temperatures of 5 K and 20 K.

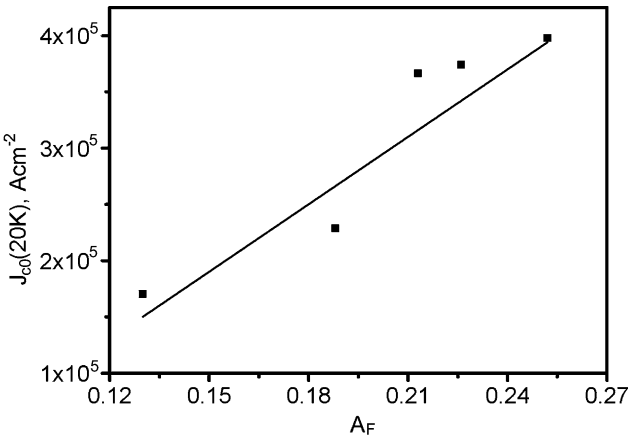

Fig. 5. Self-field J_c at 20 K vs. A_F.

As x increases from 0.9 to 1.1, J_c increases. J_c decreases when x increases from 1.1 to 1.3.

The J_c values at zero field and 20 K ($J_{c0}(20\,K)$) are listed in Table II. The correlation between $J_{c0}(20\,K)$ and A_F is shown in Fig. 5. The solid line represents the trend, as a good linear relationship can be observed. This indicates that the self-field J_c is mainly influenced by the connectivity. J_c at high field (4.6 T) and 20 K is also listed in Table II. J_c at high fields is mainly determined by the H_{c2} and the connectivity [13]. H_{c2} at 20 K, measured at 90% of the normal state resistivity, is shown in Table II. H_{c2} at 20 K as a function of microstrain is presented in Fig. 6. It is clear that H_{c2} linearly increases with microstrain. H_{c2} is determined by the disorder in MgB_2, whereas microstrain is a measure of the disorder. A lower microstrain is suggestive of a larger mean free path (l) of the superconducting electrons. This will increase the coherence length (ξ). According to $H_{c2} = \Phi_0/(2\pi\mu_0\xi^2)$, where Φ_0 is the superconducting flux quantum and μ_0 is the magnetic permeability, H_{c2} will decrease as ξ increases. It was not possible to find a monotonic relationship between H_{c2} and J_c at high field (4.6 T) and 20 K from the results listed in Table II. This implies that another factor besides

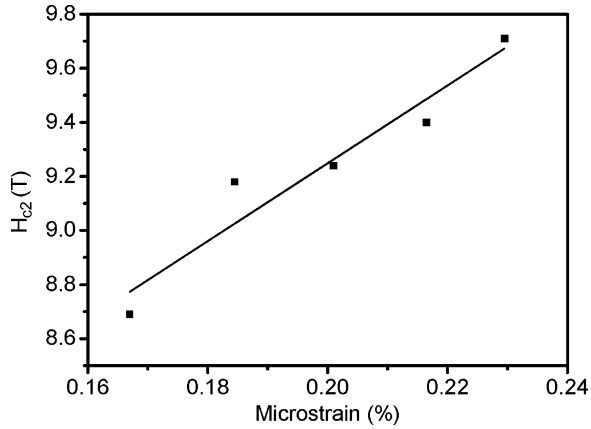

Fig. 6. H_{c2} at 20 K vs. microstrain.

H_{c2} may play a more important role in J_c at high fields. Comparing the values of J_c at 4.6 T and 20 K with the connectivity (A_F) shows that J_c increases with A_F. $Mg_{1.1}B_2$ has the largest A_F and highest J_c. Therefore, the connectivity is very likely to be the major reason for the J_c difference at high fields in the studied samples.

IV. Conclusion

Mg_xB_2 samples with $x = 0.9$, 1, 1.1, 1.2, and 1.3 were prepared by solid state reaction. Quantitative X-ray diffraction (XRD) analysis was performed to obtain the lattice constants, the microstrain, and the weight fraction of impurities using the Rietveld method. It has been found that the fraction of pure MgB_2 phase increases from $x = 0.9$ to $x = 1.1$, and then decreases with further increases in x. The critical temperature (T_c) increases with the lattice parameter *c*. In Mg_xB_2 samples, J_c increases with x to the maximum value at $x = 1.1$ and then decreases. The higher J_c at $x = 1.1$ is attributed to the better connectivity caused by smaller amounts of impurities.

Acknowledgment

The authors thank Prof. S. X Dou and Dr. T. Silver for their fruitful discussions.

References

[1] J. Nagamatsu, N. Nakagawa, T. Muramaka, Y. Zenitani, and J. Akimitsu, "Superconductivity at 39 K in magnesium diboride," *Nature*, vol. 410, pp. 63–64, Mar. 2001.

[2] S. X. Dou, S. Soltanian, J. Horvat, X. L. Wang, S. H. Zhou, M. Ionescu, H. K. Liu, P. Munroe, and M. Tomsic, "Enhancement of the critical current density and flux pinning of MgB_2 superconductor by nanoparticle SiC doping," *Appl. Phys. Lett.*, vol. 81, p. 3419, Oct. 2002.

[3] A. Yamamoto, J. Shimoyama, S. Ueda, I. Iwayama, S. Horii, and K. Kishio, "Effects of B_4C doping on critical current properties of MgB_2 superconductor," *Supercond. Sci. Technol.*, vol. 18, pp. 1323–1328, Aug. 2005.

[4] X. Xu, J. H. Kim, M. S. A. Hossain, J. S. Park, Y. Zhao, S. X. Dou, W. K. Yeoh, M. Rindfleisch, and M. Tomsic, "Phase transformation and superconducting properties of MgB_2 using ball-milled low purity boron," *J. Appl. Phys.*, vol. 103, p. 023912, Jan. 2008.

[5] T. K. Ondo, P. Badica, Y. Nakamori, S. Orimo, K. Togano, G. Nishijima, and K. Watanabe, "MgB_2/Fe superconducting tapes made using mechanically milled powders in Ar and H_2 atmospheres," *Physica C*, vol. 426–431, pp. 1231–1237, 2005.

[6] H. L. Suo, C. Beneduce, M. Dhalle, N. Musolino, J. Y. Genoud, and R. Flukiger, "Large transport critical currents in dense Fe- and Ni-clad $\mathrm{MgB_2}$ superconducting tapes," *Appl. Phys. Lett.*, vol. 79, pp. 3116–3118, Nov. 2001.

[7] A. Gümbel, J. Echert, G. Fuchs, K. Nenkov, K. H. Muller, and L. Schultz, "Improved superconducting properties in nanocrystalline bulk $\mathrm{MgB_2}$," *Appl. Phys. Lett.*, vol. 80, pp. 2725–2727, Apr. 2002.

[8] A. Yamamoto, J. Shimoyama, S. Ueda, Y. Katsura, S. Horii, and K. Kishio, "Improved critical current properties observed in $\mathrm{MgB_2}$ bulks synthesized by low-temperature solid-state reaction," *Supercond. Sci. Technol.*, vol. 18, pp. 116–121, 2005.

[9] Y. Bugoslavsky, I. F. Cohen, G. K. Perkins, M. Polichetti, T. J. Tate, R. G. William, and A. D. Caplin, "Enhancement of the high-magnetic field critical current density of superconducting $\mathrm{MgB_2}$ by proton irradiation," *Nature*, vol. 411, pp. 561–563, May 2001.

[10] C. H. Jiang, T. Nakane, and H. Kumakura, "Superior high-field current density in slightly Mg-deficient $\mathrm{MgB_2}$ tapes," *Appl. Phys. Lett.*, vol. 87, p. 252505, Dec. 2005.

[11] O. Perner, J. Eckert, W. Häßler, C. Fischer, J. Acker, T. Gemming, G. Fuchs, B. Holzapfel, and L. Schultz, "Stoichiometry dependence of superconductivity and microstructure in mechanically alloy $\mathrm{MgB_2}$," *J. Appl. Phys.*, vol. 97, p. 056105, Feb. 2005.

[12] S. K. Chen, A. Serquis, G. Serrano, K. A. Yates, M. G. Blamire, D. Guthrie, J. Cooper, H. Wang, S. Margadonna, and L. MacManus-Driscoll, "Structural and superconducting property variations with nominal Mg non-stoichiometry in $\mathrm{Mg_xB_2}$ and its enhancement of upper critical field," *Adv. Funct. Mater.*, vol. 18, pp. 113–120, 2008.

[13] M. Eisterer, "Magnetic properties and critical currents of $\mathrm{MgB_2}$," *Supercond. Sci. Technol.*, vol. 20, pp. R47–R73, Oct. 2007.

[14] Y. Eltsev, S. Lee, K. Nakao, N. Chikumoto, S. Tajima, N. Koshizuka, and M. Murakami, "Anisotropic superconducting properties of $\mathrm{MgB_2}$ single crystals probed by in-plane electrical transport measurements," *Phys. Rev. B*, vol. 65, pp. 140501–140504, Mar. 2002.

[15] P. C. Canfield, D. K. Finnemore, S. L. Bud'ko, J. E. Ostenson, G. Lapertot, C. E. Cunningham, and C. Petrovic, "Superconductivity in dense $\mathrm{MgB_2}$ wires," *Phys. Rev. Lett.*, vol. 86, pp. 2423–2426, Mar. 2001.

[16] J. M. Rowell, "The widely variable resistivity of $\mathrm{MgB_2}$ samples," *Supercond. Sci. Technol.*, vol. 16, p. R17, 2003.

[17] J. Jiang, B. J. Senkowicz, D. C. Larbalestier, and E. E. Hellstrum, "Influence of boron powder purification on the connectivity of bulk $\mathrm{MgB_2}$," *Supercond. Sci. Technol.*, vol. 19, pp. L33–L36, July 2006.